J Mater Sci (2020) 55:15695–15708

Adsorption and heterogeneous Fenton catalytic performance for magnetic Fe_3O_4/reduced graphene oxide aerogel

Fengling Zhang[1], Xiangxin Xue[1,*], Xiaowei Huang[2], and He Yang[1]

[1] *School of Metallurgy, Northeastern University, Shenyang 110819, China*
[2] *National Engineering Research Center for Rare Earth Materials, General Research Institute for Nonferrous Metals and Grirem Advanced Materials Co., Ltd., Beijing 100088, China*

Received: 5 June 2020
Accepted: 23 August 2020
Published online:
31 August 2020

ABSTRACT

Heterogeneous Fenton system has been widely used in water treatment because of its effective degradability in a wide range of pH. A two-step hydrothermal method for the synthesis of Fe_3O_4/reduced graphene oxide (RGO) aerogel was designed as an efficient and recyclable heterogeneous Fenton catalyst for degradation of methylene blue (MB). Firstly, the Fe_3O_4 colloidal solution was synthesized by hydrothermal progress. Secondly, graphene oxide hydrogels were formed by the self-assembling and reduced to graphene during the hydrothermal reaction. Meanwhile, zero-dimensional Fe_3O_4 nanoparticles were anchored onto the graphene oxide through the colloidal coagulation effect. The obtained samples were characterized by XRD, SEM, TEM, BET, Zeta, XPS, Raman, TG, and VSM. Adsorption isotherm and kinetics of MB onto Fe_3O_4/RGO composites revealed that the maximum adsorption capacity was 163.83 mg/g, and the adsorption process confirmed to the pseudo-second-order model. The determinants of heterogeneous Fenton system including oxidant concentration, initial pH, and reaction mechanism were investigated. The studies indicated that MB degradation efficiencies increased with the initial pH increasing (pH 3–10), showing a complete degradation in alkaline condition within 60 min. It is due to that catalytic reaction mainly occurs on the solid–liquid interface, as pH values increase, the electrostatic attraction between the cationic MB molecules and the surface of Fe_3O_4/RGO increases, the enhancement of adsorptivity is helpful to improve catalytic activity. The catalyst can be easily recovered by an applied magnetic field and exhibited excellent stability after five degradation cycles.

Handling Editor: Dale Huber.

Address correspondence to E-mail: xuexx@mail.neu.edu.cn

https://doi.org/10.1007/s10853-020-05159-4

Introduction

The harmful effect of various organic pollutants in water on people's life is a pressing matter of great concern and hot topic in modern scientific researches. Advanced oxidation process (AOPs) is a promising alternative strategy for wastewater treatment, especially for persistent and refractory organic pollutants. AOPs can generate strong oxidative hydroxyl radicals in the reaction process, which can non-selective attack all types of organic compounds to mineralize, leading to completely decompose contaminants into non-toxic products [1–3]. One of the most in-depth studied AOPs is Fenton system, which has unique advantages including relatively environmentally benign, low cost, high degradation efficiency, and mild reaction conditions [4–6]. However, the traditional Fenton system is efficient only in a narrow and low pH range, the secondary pollution caused by iron sludge is difficult to remove, and the catalysts cannot be recycled, which makes the route uneconomical [6–8]. Therefore, the heterogeneous Fenton system was proposed to overcome those problems and further improve the degradation capability. It can effectively decompose organic contaminants in a wide range of pH with less iron loss, and the oxidation reactions mainly occur on the solid–liquid interface where iron immobilized onto solid phase in the form of minerals or adsorbed ions [9].

The inverse spinel Fe_3O_4 is an efficient heterogeneous catalyst and attracting increasing attention [10–12]. The octahedral position in the crystal structure of Fe_3O_4 can easily accommodate Fe^{3+} and Fe^{2+}, which makes iron elements can be reversibly reduced and oxidized during the reaction while maintaining the same structure [9, 13]. Therefore, it can function steadily without causing substantial quality loss. Besides, Fe_3O_4 can be easily separated from the reaction medium when an external magnetic field is applied [14]. However, Fe_3O_4 nanoparticles tend to aggregate into large particles during the reaction process due to strong anisotropic dipolar interaction, which causes the reduction of original specific surface area, dispersibility, and catalytic performance [15–17]. Therefore, it is necessary to anchor Fe_3O_4 nanoparticles on solid supports to preserve their unique properties. Graphene has attracted much attention due to its unique properties, such as possessing a two-dimensional lamellar structure, ultra-high specific surface area, super mechanical strength, and chemical stability [18, 19]. Graphene is also a kind of effective adsorbent for organic contaminants in water treatment that displaying strong interactions with organic chemicals due to the hydrophobic surfaces [20–22], which make it fascinating and competitive support to construct graphene-based composite materials with metal oxides due to its stability and adsorption property [23, 24]. Immobilizing Fe_3O_4 on graphene supports not only prevents the aggregation of Fe_3O_4 nanoparticles but also improves the adsorptive and catalytic activity of nanocomposites because of the synergistic effects between graphene sheets and Fe_3O_4 nanoparticles.

In this paper, the Fe_3O_4 superparamagnetic colloidal solution was synthesized firstly, and then the zero-dimensional Fe_3O_4 nanoparticles were fastened to the three-dimensional framework of graphene aerogel by a simple, mild, and low-cost hydrothermal method. The Fe_3O_4 colloid nanoparticles could bind with graphene oxide by electrostatic interaction, and the whole self-assembly process can be accomplished by colloidal coagulation effect (CCE) without any linker as assistants. This work makes the classical CCE successfully extend to the application of assembling Fe_3O_4 nanoparticles on graphene and realizes Fe_3O_4 nanoparticles distributed uniformly on graphene sheets without chemical structure changed. The adsorption and catalytic properties of Fe_3O_4/reduced graphene oxide (RGO) were studied systematically. In this article, the as-prepared Fe_3O_4/RGO nanocomposites were used as adsorbent and heterogeneous Fenton catalyst to degrade a very common cationic dye methylene blue (MB), and the formation mechanism was discussed.

Experimental method

Synthesis of Fe_3O_4/RGO nanocomposites

Preparation of graphene oxide (GO) by a modified Hummers method [25], which can be briefly described as follows: Graphite powder (1 g) and $NaNO_3$ (0.5 g) were successively added into concentrated H_2SO_4 (23 ml) solution with thorough ice bath stirring, and then solid $KMnO_4$ (3 g) was put slowly into the beaker. After being kept at 0 °C for 4 h, the mixture was stirred at 40 °C until it turned brownish paste and slowly diluted with deionized water while the reaction temperature raising to 98 °C and remained for 15 min. Then, slowly added H_2O_2 (30%, 10 ml) and the color of the mixture became brilliant yellow. At last, the mixture was washed with 5wt% HCl aqueous and distilled water in order to remove residual metal ions and acid, and the synthesized graphene oxide suspension was obtained after ultrasonic treatment for 30 min (40 kHz, 400 W).

Fe_3O_4 nanoparticles were synthesized via a hydrothermal method. Concretely, $FeCl_3$ (0.5 g) was added into the mixture of distilled water (20 ml) and ethylene glycol (40 ml) with magnetic stirring. Then NaOH (1.6 g) was added and stirred to dissolve completely. After that, the mixed homogeneous solution was transferred into Teflon stainless-steel autoclave and reacted at 180 °C for 12 h. Then, the obtained Fe_3O_4 nanoparticles were thoroughly water-washed by centrifugation at 10,000 rpm until the pH of the solution was near neutral. The resulting product was dispersed in deionized water without any additives to obtain a colloidal solution by ultrasonic treatment for 10 min (40 kHz, 200 W).

Fe_3O_4/RGO hydrogels were formed by hydrothermal process. The above Fe_3O_4 colloidal solution (30 ml) was separately added into GO solution (40 ml) with different mass ratios (30 wt%, 50 wt%, 70 wt%) to obtain homogeneous colloidal coagulation by mechanical agitation, then transferred into 100-ml Teflon stainless-steel autoclave, and reacted at 120 °C for 24 h. For comparison purposes, RGO was also prepared in similar procedures in the absence of Fe_3O_4. The obtained RGO, Fe_3O_4/RGO hydrogels, and Fe_3O_4 colloidal solution were freeze-dried treatment at − 45 °C for 48 h. In this preparation process, the samples with different Fe_3O_4 contents (including 0, 30, 50, 70, 100 wt%) were prepared, as defined RGO, Fe_3O_4/RGO-1, Fe_3O_4/RGO-2, Fe_3O_4/RGO-3, and Fe_3O_4, respectively.

Characterization

The crystal structure was investigated by X-ray powder diffraction (Philips X'Pert PRO, Netherlands). The morphology features were studied with field emission scanning electron microscopy (Zeiss Ultra, German) and transmission electron microscopy (JEM2100, Japan). N_2 adsorption/desorption measurements were taken with an Autosorb IQ gas sorption system (Quantachrome, USA). Zeta potentials were measured on a Malvern Zetasizer Nano system (ZS90, UK). Chemical valence was analyzed by X-ray photoelectron spectroscopy (ESCALAB250, England). The Raman spectra were measured at 514-nm excitation with an in Via Laser Raman Spectrometer (HR800, France). Thermal gravimetric analysis (SDT2960, American) was carried out under air atmosphere from room temperature to 800 °C with a heating rate of 10 °C min^{-1}. The magnetic property was measured with a maximum applied magnetic field of 18KOe by a vibrating sample magnetometer (LS74035, USA) at room temperature. The UV–Vis diffuse reflectance spectra at a wavelength of 664 nm were recorded by a UV–Vis absorption spectrometer (UV2550, Japan).

Adsorption isotherms and kinetics

Adsorption isotherm experiments were carried out at 25 °C, and 15 mg samples (RGO, Fe_3O_4/RGO-1, Fe_3O_4/RGO-2, and Fe_3O_4/RGO-3) were individually added into a conical flask containing an initial MB aqueous solution concentration (40–100 mg/L, 50 ml). The flasks were shaken for 48 h in an oscillating incubator (SPX-150B-D, China) to ensure the adsorption equilibrium. Then the amount of MB adsorbed at equilibrium concentration and the removal percentage were calculated according to:

$$q_e = \left(\frac{C_0 - C_e}{m}\right) \times V \quad (1)$$

$$\text{Removal Percentage } (\%) = \frac{C_0 - C_t}{C_0} \times 100\% \quad (2)$$

where q_e (mg/g) is the equilibrium adsorption capacity, C_0 (mg/L), C_e (mg/L), and C_t (mg/L) are the concentration of MB at initial, equilibrium, and at time t, respectively; V (mL) is the volume of solution, and m (g) is the mass of solid sorbent.

The kinetic adsorption experiment was carried out by adding Fe_3O_4/RGO-2 (30 mg) to MB aqueous solutions (50 mg/L, 100 ml) with mechanically stirring. At predetermined moments the concentration of MB aqueous solution was determined spectrophotometrically. The adsorption capacity of MB at time t was calculated according to the following equation:

$$q_t = \left(\frac{C_0 - C_t}{m}\right) \times V \quad (3)$$

where q_t (mg/g) is the adsorption capacity at time t.

Degradation experiment

The heterogeneous Fenton reaction was studied by monitoring the degradation of MB in a beaker (250 ml) with a mechanical agitator. The experiments were started by adding 30 mg catalyst (Fe_3O_4/RGO-1, Fe_3O_4/RGO-2, Fe_3O_4/RGO-3, and Fe_3O_4) into MB aqueous solution (50 mg/L, 100 ml) and ultrasound 10 min to accelerate the adsorption/desorption equilibrium. Then, the catalytic reaction was stimulated by adding H_2O_2 solution (30 wt%). At a predetermined time interval, 5 mL solution was extracted and centrifuged to measure MB concentration. Batch experiments were carried out to study the effects of catalysts, initial pH (adjusting by adding HCl and NaOH), the concentration of H_2O_2 solution on the degradation of MB and confirm the catalytic mechanism. The degradation efficiency (η) of MB was calculated by the following equation:

$$\eta = \frac{C_0 - C_t}{C_0} \times 100\% \quad (4)$$

Results and discussion

Schematic diagram for preparation of Fe_3O_4/RGO aerogels

As shown in Fig. 1, the whole reaction process was accomplished by a mechanism similar to the colloidal coagulation effect (CCE), and coagulation can cause by the electrostatic interactions between colloidal particles and ions with opposite charges in solution. The graphene oxide (GO) obtained through wet-chemical oxidation method served as the ions, and the colloidal coagulation process began to be driven by electrostatic interactions when they were mixed together with Fe_3O_4 colloid nanoparticles [26]. Through hydrothermal treatment, the GO was self-assembled and reduced to graphene, while Fe_3O_4 nanoparticles anchored on the hydrogel, and after freeze-drying treatment the Fe_3O_4/RGO three-dimensional aerogels were formed.

Characterization analysis

The crystalline structures of synthesized samples were identified by X-ray diffraction. Figure 2a shows a characteristic peak at 2θ = 10.8° corresponds to the diffraction peak of GO. After the hydrothermal process, GO diffraction peak disappeared completely with the formation of RGO characteristic peak at 2θ = 23.9° (Fig. 2b) [27]. As seen in Fig. 2d–f, the peaks at 2θ values of 18.33°(1 1 1), 30.16°(2 2 0), 35.52° (3 1 1), 43.17° (4 0 0), 53.56° (4 2 2), 57.10° (5 1 1), and 74.19° (5 3 3) were consistent with the standard XRD data for the inverse spinel structure Fe_3O_4 (JCPDS card 01–088-0315), and this indicated that the Fe_3O_4 crystal structure was not destroyed in the hydrothermal synthesis of nanocomposites. There was an obvious diffraction peak assigned to reduced graphene oxide in Fe_3O_4/RGO-1 due to the high mass ratio (Fig. 2c).

As shown in Figs. 1 and 3a, the graphene nanosheets are assembled to macroscopic three-dimensional structure during hydrothermal process. Obviously, such a structure is not only suitable for the exposure of Fe_3O_4 nanoparticles, but also facilitated to the adsorption and diffusion of reactants in the catalytic

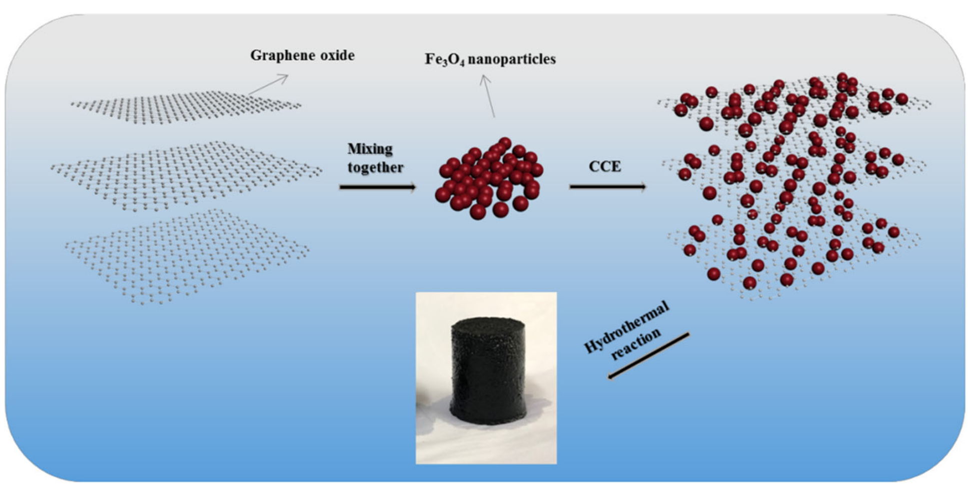

Figure 1 Schematic diagram for hydrothermal synthesis of Fe_3O_4/RGO hydrogel.

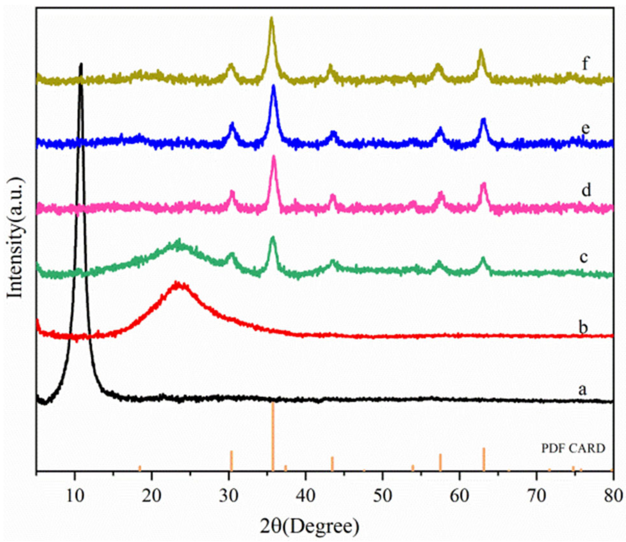

Figure 2 XRD patterns of GO (a), RGO (b), Fe_3O_4/RGO-1 (c), Fe_3O_4/RGO-2 (d), Fe_3O_4/RGO-3 (e), and Fe_3O_4 (f).

reaction. Figure 3b shows that the Fe_3O_4 nanoparticles were easily aggregate together to form chains structure. After the formation of Fe_3O_4/RGO-2 aerogels (Fig. 3c), the Fe_3O_4 nanoparticles without aggregation were uniformly anchored on the graphene nanosheets, and the EDS elemental mapping result (Fig. 3d and Fig. S1) illustrated the homogeneous existence of Fe, O, and C in the nanocomposites. TEM images (Fig. 3e, f) further confirmed the uniform particle size of the Fe_3O_4 nanoparticles with an average particle size of (10–20) nm was evenly dispersed and immobilized on the graphene sheets.

To gain further insight into the porous properties of the samples, nitrogen adsorption–desorption measurements were measured. The N_2 adsorption/desorption isotherms of the samples displayed a type IV isotherm with a hysteresis loop in the range of $P/P_0 = 0.4 - 1.0$ (Fig. S2), indicating the existence of

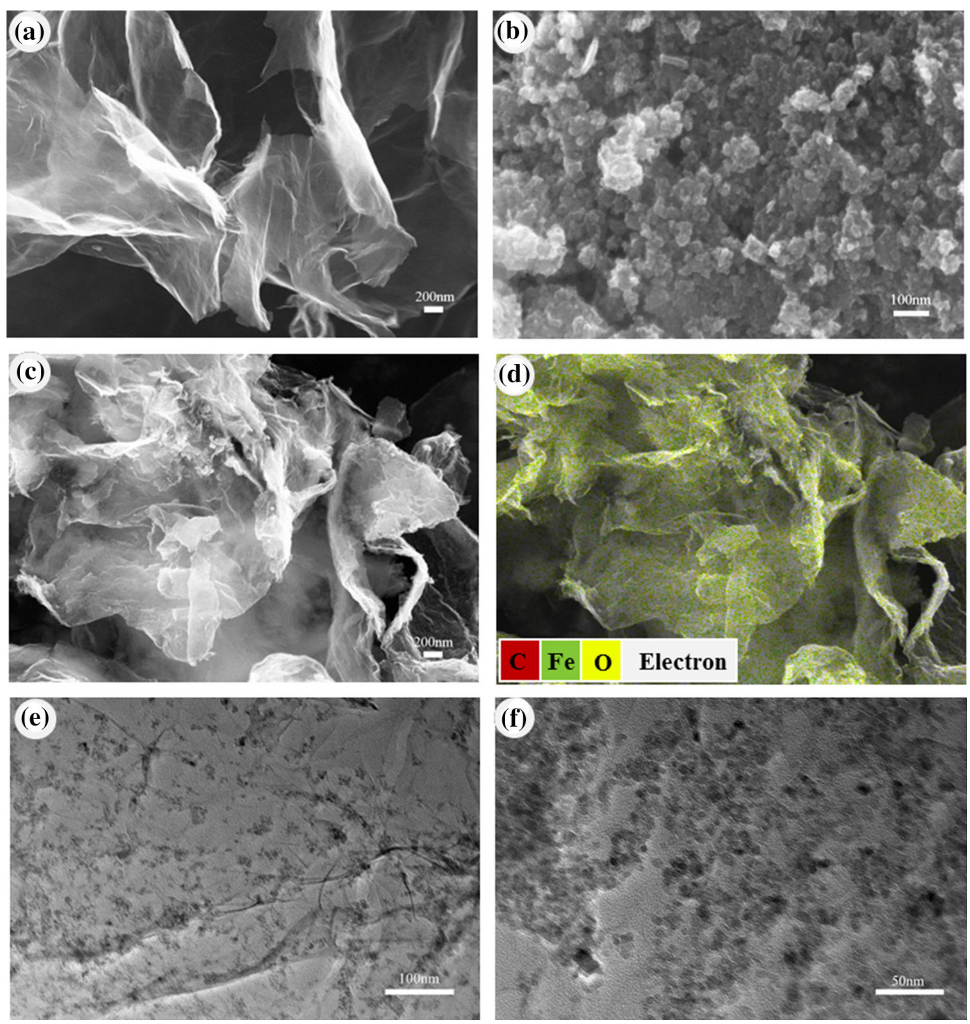

Figure 3 SEM images of RGO (**a**), Fe_3O_4 nanoparticles (**b**), Fe_3O_4/RGO-2 (**c**), and EDS elemental mapping of Fe_3O_4/RGO-2 (**d**); TEM images of microstructure of Fe_3O_4/RGO-2 (**e**, **f**) at different magnifications.

abundant mesopores [24]. The Fe_3O_4/RGO-2 had a BET-specific surface area up to 200.40 m^2/g, a little higher than RGO (172 m^2/g) but much higher than pure Fe_3O_4 (15.57 m^2/g). With the increase of Fe_3O_4 mass loading, the specific surface area of Fe_3O_4/RGO-1 and Fe_3O_4/RGO-3 was 170 m^2/g and 145.9 m^2/g, respectively, which distributed among those of RGO and Fe_3O_4. This indicated that appropriate mass loading of Fe_3O_4 nanoparticles could prevent the aggregation of RGO to a certain degree, while excess Fe_3O_4 would cause relatively restacking and smaller the specific surface area [28]. The DFT pore size distributions (Fig. S2) of all samples were composed of a peak ranging between 2 and 50 nm, proving the existence of a highly mesoporous structure [29]. The large surface area and highly developed porosity are beneficial to increase the adsorption properties of nanocomposites.

Zeta potential analysis is an important indicator to characterize the stability of dispersions, and the surface charges of the samples were highly negatively charged when dispersed in water (Fig. S3). The zeta potential of RGO was − 36.7 mV, and with the increase of Fe_3O_4 dosage, the zeta potential of nanocomposites increased first and then decreased. The zeta potential of Fe_3O_4/RGO-1, Fe_3O_4/RGO-2, Fe_3O_4/RGO-3 was − 28.4 mV, − 40.3 mV, and − 43.7 mV, respectively, which suggested the stability of their dispersions gradually improved [30]. By correlating the zeta potential of Fe_3O_4/RGO-2 with the initial pH values, it can be found that acid condition corresponded to a higher zeta potential, while the higher pH had a lower zeta potential, and the alkali condition made the surface charges of the nanocomposites become more negative. Highly negatively charged in suspension could not only improve the electrostatic attraction with the cationic MB molecules, but also disperse homogeneously via electrostatic repulsion [31, 32].

The prepared Fe_3O_4/RGO-2 nanocomposites were further examined by XPS spectroscopy to get the important information of electronic structure and chemical composition. As shown in Fig. 4a, the wide scan XPS spectrum confirmed the presence of C, O, and Fe elements with binding energy at 285 eV (C1s), 530 eV (O1s), and 711Ev (Fe 2p), respectively [33]. From the Fe2p spectrum in Fig. 4b, the two peaks located at 711 eV and 724.5 eV belonging to the Fe2p3/2 and Fe2p1/2 spin–orbit characteristic peaks of Fe_3O_4 [34]. The C1s spectrum (Fig. 4c) showed the peak at 284.6 and 286.1 eV, which were attributed to non-oxygenated C (C–C/C=C) in aromatic rings, and the C in C–O of epoxy and alkoxy [35]. The O1s peak of Fe_3O_4/RGO-2 (Fig. 4d) contained three types of oxygen species. The peak at 530.4 eV arose from Fe_3O_4, while the peak at 533 eV was assigned to the residual oxygen in graphene sheets. The peak at 531.7 eV might come from the bonds between Fe_3O_4 and graphene and/or cause by the C=O group. However, C=O peak was not detected in C1s, so the peak at 531.7 eV in the spectrum was attributed to the covalent bond of Fe–O–C formed by the attachment of Fe_3O_4 nanoparticles onto graphene sheets [36].

Raman spectroscopy is a useful tool to analyze the order of crystal structures of carbon materials. Figure 5a shows the spectra curves of GO, RGO, and Fe_3O_4/RGO-2; there were two characteristic peaks appearing at 1340 cm^{-1} and 1590 cm^{-1}, which correspond to D band and G band, respectively. The D band is related to the structural defects in disordered carbon, while the G band is the E_{2g} vibration mode of the first-order scattering in *sp*2 carbon domains [37, 38]. The intensity ratio (I_D/I_G) is usually associated with the disorder of carbon [39]. Compared with GO, the Fe_3O_4/RGO-2 showed an enhanced value of I_D/I_G, indicating there were more *sp*3 defects in the *sp*2 carbon network during the formation of Fe_3O_4/RGO-2 nanocomposites. The content of each component in the sample can be conveniently determined by thermogravimetric analysis via oxidative decomposition. As shown in Fig. 5b, the mass content of the graphene in the Fe_3O_4/RGO-2 was evaluated to be 48.31 wt%, which is close to the preset value of the experiment (50 wt%).

The saturation magnetization (Ms) value of Fe_3O_4/RGO-2 aerogel (34.4 emu/g) was (Fig. 6) smaller than the bulk magnetite (92 emu/g). It is mainly attributed to smaller particle size and the existence of nonmagnetic graphene [40]. The hysteresis loop of the Fe_3O_4/RGO-2 was S-shaped with negligible coercivity and remanence, indicating that it had superparamagnetic nature, which was benefit to recover from the reaction solution by an external magnetic field [41].

Adsorption kinetics and isotherms analysis

The adsorption isotherm is an important parameter to evaluate an equilibrium adsorption process and assess the capacity of an adsorbent at a fixed

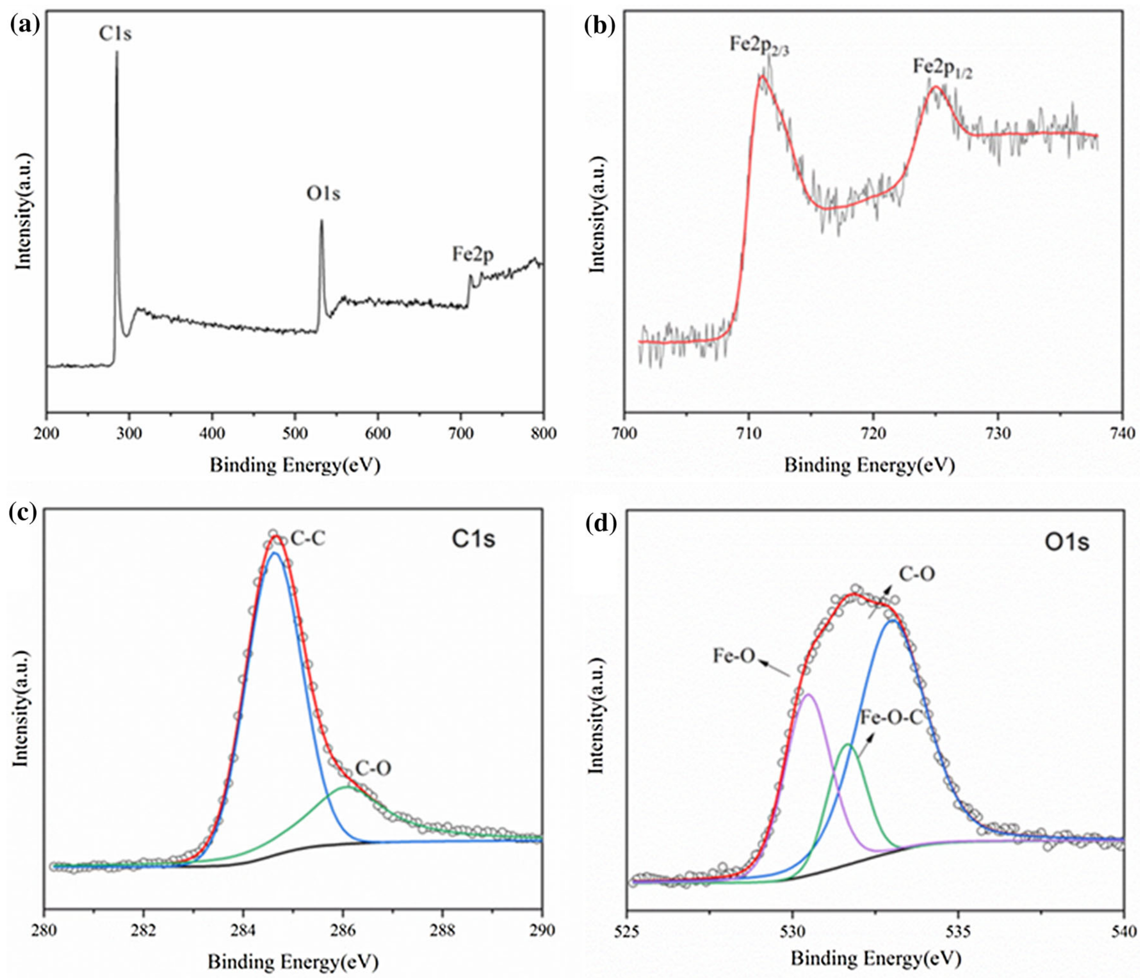

Figure 4 XPS survey spectra of Fe_3O_4/RGO-2 (**a**) full range, (**b**) Fe2p, (**c**) C1s, (**d**) O1s.

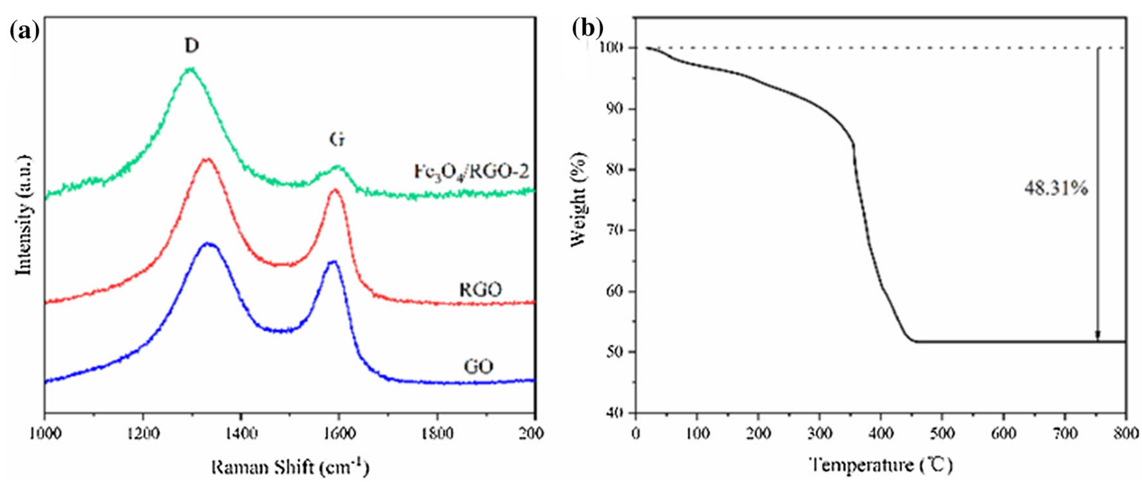

Figure 5 Raman spectra of samples (**a**) and TG curve of Fe_3O_4/RGO-2 (**b**).

temperature. The adsorption isotherms of MB on samples at room temperature (pH 7) were listed (Fig. 7a and Fig. S4), and the fitting result models are given in Table 1. The Langmuir model is based on the assumption that the monolayer adsorption process occurs on uniform surfaces [42], while the Freundlich

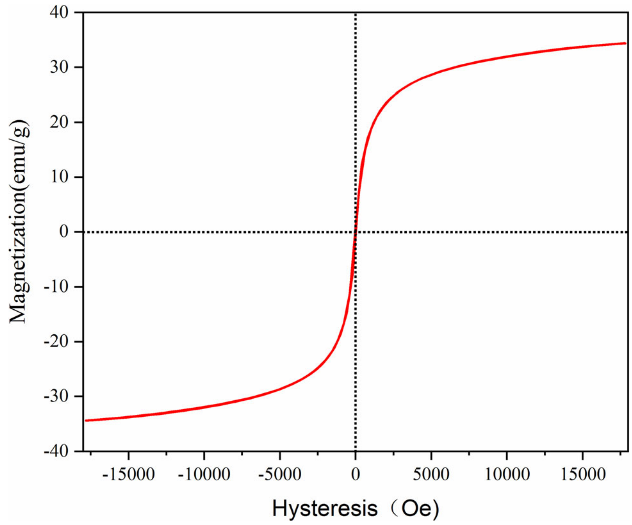

Figure 6 Hysteresis loop for the synthesized Fe_3O_4/RGO-2.

isotherm, which presumes that adsorption is located on the multilayer and adsorption sites on the adsorbent, is heterogeneous [43]. The two nonlinear adsorption isotherm models can be described as follows [44]:

$$q_e = \frac{Q_m b C_e}{1 + b C_e} \tag{5}$$

$$q_e = K_F C_e^{1/n} \tag{6}$$

where Q_m (mg/g) and b (L/mg) are the Langmuir constants related to adsorption capacity and adsorption rate. K_F (L/mg) and n are Freundlich constants. It is observed that with the increase of (Fe_3O_4)/(RGO) ratios, the adsorption properties of the samples increased first and then decreased, and the maximum adsorption capacities of RGO, Fe_3O_4/RGO-1, Fe_3O_4/RGO-2, and Fe_3O_4/RGO-3 were 110.0549, 158.7451, 163.8256, and 111.2981 mg/g, respectively. The main reason is that the introduction of Fe_3O_4 nanoparticles could lower the stacking of graphene nanosheets during self-assemble process, while excessive Fe_3O_4 nanoparticles agglomerate on the surface of graphene will decrease the specific surface area and porosity of the nanocomposites, thus reducing the active sites. The maximum adsorption capacity of our prepared material is compared with other materials previously

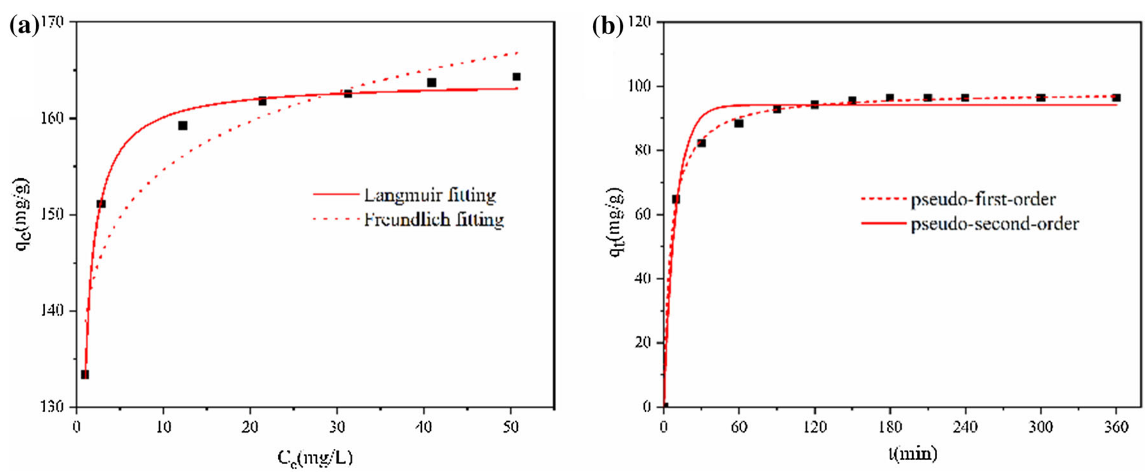

Figure 7 Adsorption isotherms (**a**) and kinetics (**b**) for MB on Fe_3O_4/RGO-2.

Table 1 Isotherm parameters on removal of MB

Sample	Langmuir			K_F	Freundlich		
	Q_m	b	R^2		n	R^2	R_L
RGO	110.0549	0.1763	0.9962	55.3913	0.1466	0.9405	0.0537–0.1242
Fe_3O_4/RGO-1	158.7451	2.5104	0.9919	132.5457	0.0487	0.8698	0.0039–0.0099
Fe_3O_4/RGO-2	163.8256	4.3162	0.9923	138.8919	0.0466	0.8731	0.0023–0.0058
Fe_3O_4/RGO-3	111.2981	0.3039	0.9952	70.2128	0.1008	0.9258	0.0319–0.0760

reported and presented in Supplementary Table. S1. It can be observed that the performance of Fe_3O_4/RGO-2 fares well in comparison with the adsorbents available in the current literature. The removal percentage decreased with the increase of MB initial concentration (Fig. S5). This may be due to the availability of more active sites on the surface of the adsorbent for dye adsorption at a lower dye concentration, while the binding sites of dye molecules are saturated at a higher dye concentration. Fitting results showed the correlation coefficients (R^2) of Langmuir isotherm were higher than that of Freundlich isotherm, which meant that the Langmuir isotherm model was more suitable for describing the adsorption behavior, and the monolayer adsorption was proposed.

The feasibility of adsorbent adsorption was evaluated by the separation factor (R_L) associated with Langmuir isotherm. It can be calculated by the following equations [45]:

$$R_L = \frac{1}{1 + bC_0} \tag{7}$$

The R_L values were in the range ($0 < R_L < 1$) (Table 1), indicating that MB adsorption on the samples was favorable [46].

Adsorption kinetic studies were explored to understand MB adsorption behavior on the Fe_3O_4/RGO-2. As shown in Fig. 7b, in the first 60 min, the adsorption capacity increased rapidly with prolonging the contact time, and then the adsorption rates slowed down gradually until reaching the equilibrium within 3 h. The adsorption mechanism was further investigated by the pseudo-first-order (Eq. 8) and pseudo-second-order (Eq. 9) kinetic equations, which were expressed in a nonlinear form [32]:

$$q_t = q_e(1 - e^{-k_1 t}) \tag{8}$$

$$q_t = \frac{q_e^2 k_2 t}{1 + q_e k_2 t} \tag{9}$$

where q_e and q_t (mg/g) are the adsorption amount of MB at equilibrium and time t. k_1 is the pseudo-first-order rate constant, and k_2 (mg/g/s) is the pseudo-second-order rate constant. k_1 and k_2 (mg/g/s) are rate constants of pseudo-first-order and pseudo-second-order, respectively. As displayed in Table 2, the R^2 value of pseudo-second-order model was higher, and the experimental q_e value (96.4 mg/g) fit more closely to the pseudo-second-order than the pseudo-first-order model [44], which indicated that the adsorption process confirmed to the pseudo-second-order model.

Catalytic activity of Fe_3O_4/RGO nanocomposites

A series of contrast experiments were carried out to investigate the heterogeneous Fenton catalytic activity of the Fe_3O_4/RGO nanocomposites. As seen in Fig. 8a, the degradation efficiency of MB was only 31% in the presence of Fe_3O_4 alone, which can be due to the low adsorption capacity and slow reactivity on the surface of Fe_3O_4. Compared with Fe_3O_4 nanoparticles, the Fe_3O_4/RGO nanocomposites showed more effective MB degradation. With the increase of (Fe_3O_4)/(RGO) ratios, the degradation efficiency of the samples increased first and then decreased. This is mainly owing to the synergistic effect between Fe_3O_4 and RGO. The dynamic equilibrium process discussed indicated that the adsorption MB molecules were very quick and easy. The high concentration of MB molecules adsorption on RGO support near the active catalytic center of Fe_3O_4 was vulnerable to attack by the generated ·OH [9]. In the initial stage of the degradation reaction, this favorable effect was relatively obvious. However, excessive Fe_3O_4 nanoparticles anchored on the graphene nanosheets would show low adsorption capacity and slow reactivity.

The oxidant concentration is an important factor affecting the degradation efficiency in the Fenton oxidation system. The effect of H_2O_2 concentration on MB degradation is shown in Fig. 8b and Fig. S6. The dosage range of H_2O_2 increased from 0 to 15 mmol, and the degradation rate was significantly improved. However, when the H_2O_2 concentration was increased to 20 mmol, it showed that the degradation

Table 2 Coefficients of adsorption kinetic models

Sample	Pseudo-first-order			Pseudo-second-order		
	$q_{e,cal}$	k_1	R^2	$q_{e,cal}$	k_2	R^2
Fe_3O_4/RGO-2	94.1978	0.1065	0.9824	98.3532	0.0019	0.9990

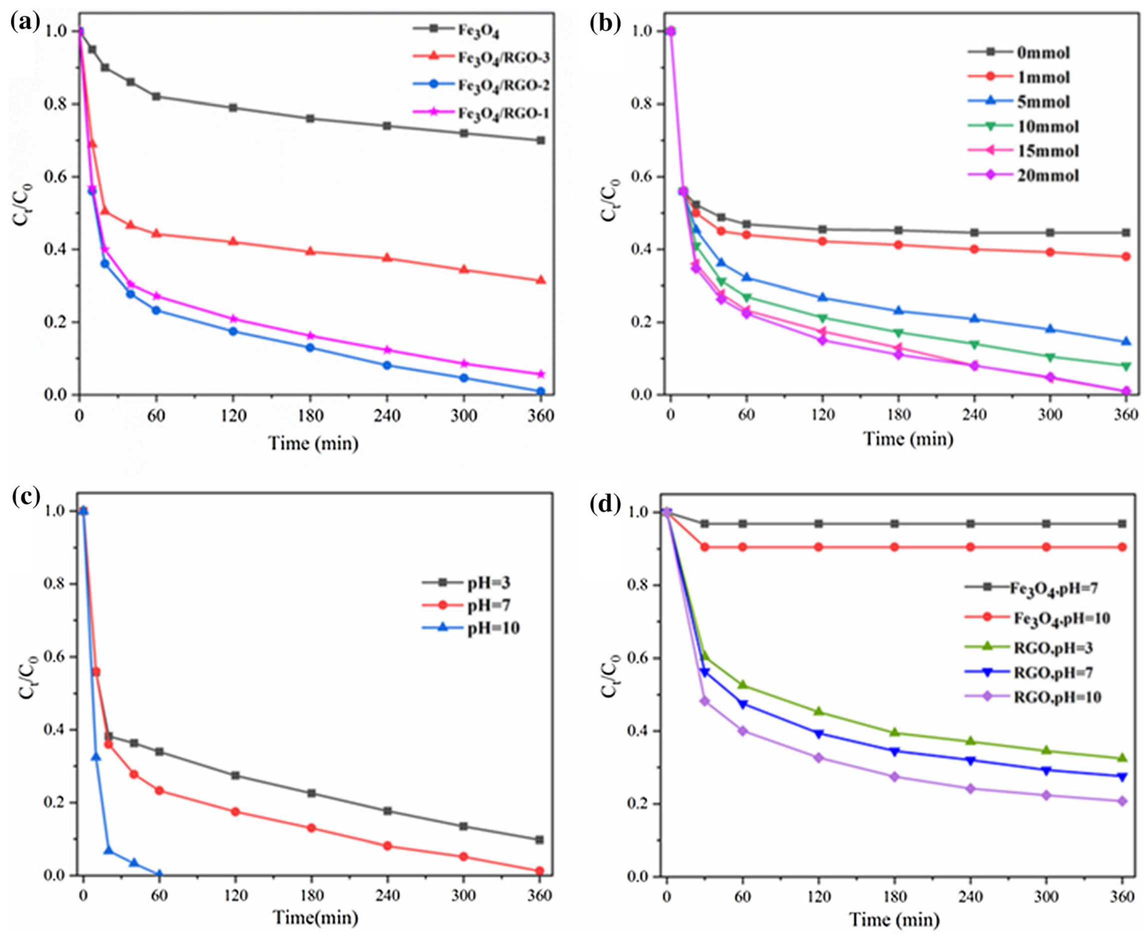

Figure 8 Effect of operating parameters on MB degradation in the heterogeneous Fenton system: **a** different catalysts, **b** H_2O_2 dosage, **c** initial pH value, **d** adsorption properties for RGO and Fe_3O_4 without H_2O_2 at different pH. Except for the investigated parameter, other parameters fixed on pH 7.00, [MB] = 50 mg/L, [catalyst] = 0.30 g/L, [H_2O_2] = 15 mmol, and T = 25 °C.

ability not enhanced with the H_2O_2 further increase. This phenomenon indicated that excess H_2O_2 played as a scavenger for hydroxyl radicals (·OH), and the generating hydroperoxyl radical (·OOH) (Eq. 10) had much lower oxidation capabilities and could further consume the ·OH (Eq. 11) [47, 48].

$$H_2O_2 + \cdot OH \rightarrow \cdot OOH + H_2O \quad (10)$$

$$\cdot OOH + \cdot OH \rightarrow H_2O + O_2 \quad (11)$$

Fe(II) mainly exists in the form Fe^{2+} at a low pH range (pH < 3) and would change into $Fe(OH)^+$ and $Fe(OH)_2$ when pH values increase to 4 [49, 50]. Consequently, traditional Fenton reaction is effective just in the range of acidic pH, while the ·OH radical has a fairly strong oxidation ability under acidic conditions. Effect of initial pH value of solution on the catalytic performance was investigated by a set of degradation experiments. As shown in Fig. 8c, the degradation rate of MB decreased with the increase of pH value. In the initial alkaline condition, the system showed the best of degradation efficiency of 100% with 60 min. However, the degradation efficiency reduced to 66.08% and 76.73% in 60 min under initial acidic and neutral conditions. The main reasons are as follows: Firstly, the heterogeneous Fenton oxidation reactions mainly occur on the solid–liquid interface, and the enhancement of adsorptivity is helpful to improve catalytic activity [9]. Secondly, the change of solution pH has an effect both on the surface charge of adsorbent and the functional groups on the active sites. This can be demonstrated in Fig. 8d, at acidic condition, competitive adsorption existed between the presence of excess H^+ and cationic MB dye molecules on the available adsorption sites of RGO surface. As the pH value increased, the electrostatic attraction between MB molecules and RGO surface increased, resulting in the enhancement of dye adsorption [27, 51]. When the pH was beyond 7, the main reasons for the relatively higher absorptivity could be as follows: (1) Under alkaline condition, the generating $Fe(OH)_3$ on the surface of Fe_3O_4 catalyst has good adsorption and precipitation ability [49]; (2) the electrostatic attraction between the cationic MB and negatively charged graphene sheets further increased [31]. A summary of the catalytic activities of some published Fe_3O_4-based catalysts on the degradation of MB dye is presented in Supplementary Table. S2. It can be clearly observed that Fe_3O_4/RGO-2 catalyst is well comparable to other studied catalysts, whether activation method, catalyst dosage, MB concentration, or reaction time.

Reusability is also one of the most critical factors affecting the catalyst application. Successive experiments were performed to investigate the reusability of Fe_3O_4/RGO-2. After heterogeneous Fenton catalytic degradation, Fe_3O_4/RGO-2 was removed from the solution by an external magnetic field and washed with deionized water for the next degradation experiment. The degradation cycles of MB are presented in Fig. 9, and the corresponding UV–Vis absorption spectra are provided in Fig. S7. The degradation efficiency can maintain 96.60% for five degradation processes, which indicated excellent reusability of Fe_3O_4/RGO-2.

Mechanism discussion

To verify whether the catalytic reaction in heterogeneous Fenton process was initiated by leaching iron or on the surface of the catalyst, H_2O_2 was added into the Fenton system after the Fe_3O_4/RGO-2 nanocomposites removing from the adsorption equilibrium solution and started the Fenton reaction. As seen from Fig. 10, the degradation rate of homogeneous Fenton system was only 3.4% in 360 min under the same experimental conditions, much lower than the Fe_3O_4/RGO-2 heterogeneous system, indicating that the heterogeneous oxidation of the MB mainly occurs on the catalyst's surface. To confirm the catalytic mechanism, *t*-butanol (TBA) was added as radical scavengers before reaction to identify the hydroxyl radicals generated from the decomposition of H_2O_2 catalyzed by Fe_3O_4/RGO-2 catalyst. The presence of TBA remarkably suppressed the MB degradation (Fig. 10), which indicated that hydroxyl radicals (·OH) played an important role in the catalytic degradation of MB for Fe_3O_4/RGO-2 heterogeneous Fenton system.

From the above analysis, the possible degradation process can be described as follows (Fig. 11):

$$Fe(II) + H_2O_2 \rightarrow Fe(III) + OH^- + \cdot OH \quad (12)$$

$$Fe(III) + H_2O_2 \rightarrow Fe(II) + \cdot OOH + H^+ \quad (13)$$

$$Fe(III) + \cdot OOH \rightarrow Fe(II) + O_2 + H^+ \quad (14)$$

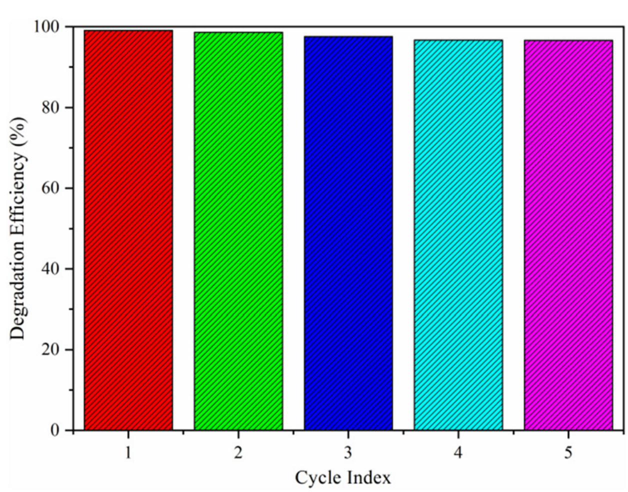

Figure 9 The degradation efficiency of Fe_3O_4/RGO-2 for five times cycle. Experimental conditions: [MB] = 50 mg/L, [Fe_3O_4/RGO-2] = 0.3 g/L, [H_2O_2] = 150 mmol, initial pH 7.

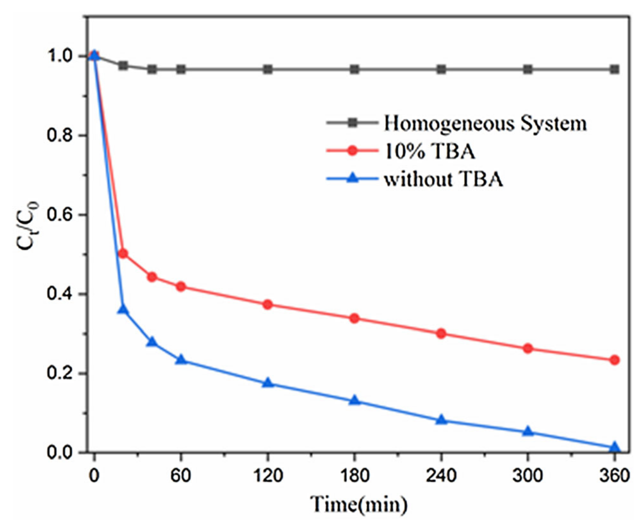

Figure 10 Effects of t-butanol and leaching iron on Fenton system. Experimental conditions: [MB] = 50 mg/L, [Fe_3O_4/RGO-2] = 0.3 g/L, [H_2O_2] = 150 mmol, initial pH 7.

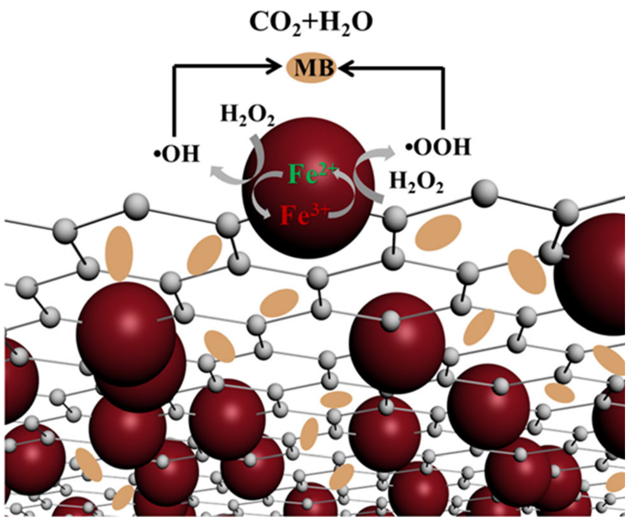

Figure 11 Schematic diagram for the Fe_3O_4/RGO heterogeneous Fenton system.

In the Fe_3O_4/RGO-2 heterogeneous Fenton system, the dominant reaction begins with MB molecules adsorption onto the Fe_3O_4/RGO-2 surface, followed by a chain of degradation reactions. The Fe^{2+} and H_2O_2 on the surface of the Fe_3O_4/RGO-2 nanocomposites initiate the heterogeneous Fenton reaction via classical Haber–Weiss mechanism (Eq. 12) [48], and the Fe^{2+} could be regenerated by Eqs. (13)–(14) [5, 52]. Once the adsorbed MB dye molecules are degraded, the adsorption equilibrium is broken. More MB molecules would transfer from solution to the surface of Fe_3O_4/RGO-2 and react with ·OH through a series of redox reactions to form CO_2, H_2O, and other intermediates. The graphene served as supporter has also played a vital role in this process: It not only increases the Fe_3O_4/RGO-2 nanocomposites surface area but also makes cationic MB molecules could be easily adsorbed on catalyst surface because of the electrostatic attraction between cationic MB and negatively charged surface graphene, and the π–π interaction between the aromatic rings of graphene and MB molecules [53], thus improving the adsorption performance of the Fe_3O_4/RGO-2.

Conclusion

In this study, a facile hydrothermal approach was proposed to anchor zero-dimensional Fe_3O_4 nanoparticles on the three-dimensional framework of graphene aerogel through the colloidal coagulation effect. Adsorption isotherms and kinetics showed that Fe_3O_4/RGO-2 had high adsorption capacity. The adsorption process followed the pseudo-second-order kinetic model, and Langmuir isotherm model was more suitable for describing the adsorption behavior. The heterogeneous Fenton reaction indicated the oxidation process mainly occurred on the surface of Fe_3O_4/RGO-2 with negligible leaching iron. The enhanced catalytic activity in the oxidation reaction was attributed to the positive effect of graphene adsorption on dye molecules, which promoted the degradation rate, benefiting from the synergetic effect of zero-dimensional Fe_3O_4 nanoparticles and three-dimensional network of graphene nanosheets, making Fe_3O_4/RGO-2 a very attractive adsorbent and heterogeneous Fenton catalyst. Furthermore, the unique assembly route to form Fe_3O_4/RGO aerogel may provide an alternative way for selective synthesis of graphene-based metal compounds for special applications.

Acknowledgements

This work was supported by the National Natural Science Foundation of China (U1261120).

Compliance with ethical standards

Conflict of interest The authors declare no conflict of interest.

Electronic supplementary material: The online version of this article (https://doi.org/10.1007/s10853-020-05159-4) contains supplementary material, which is available to authorized users.

References

[1] Jiao Y, Wan C, Bao W, Gao H, Liang D, Li J (2018) Facile hydrothermal synthesis of Fe3O4@cellulose aerogel nanocomposite and its application in Fenton-like degradation of Rhodamine B. Carbohyd Polym 189:371–378

[2] Yang B, Tian Z, Zhang L, Guo Y, Yan S (2015) Enhanced heterogeneous Fenton degradation of methylene blue by nanoscale zero valent iron (nZVI) assembled on magnetic Fe3O4/reduced graphene oxide. J Water Process Eng 5:101–111

[3] Hua Z, Ma W, Bai X, Feng R, Yu L, Zhang X, Dai Z (2014) Heterogeneous Fenton degradation of bisphenol A catalyzed

by efficient adsorptive Fe3O4/GO nanocomposites. Environ Sci Pollut Res Int 21(12):7737–7745

[4] Yu L, Chen J, Liang Z, Xu W, Chen L, Ye D (2016) Degradation of phenol using Fe3O4-GO nanocomposite as a heterogeneous photo-Fenton catalyst. Sep Purif Technol 171:80–87

[5] Cleveland V, Bingham J-P, Kan E (2014) Heterogeneous Fenton degradation of bisphenol A by carbon nanotube-supported Fe3O4. Sep Purif Technol 133:388–395

[6] Guo S, Zhang G, Guo Y, Yu JC (2013) Graphene oxide–Fe2O3 hybrid material as highly efficient heterogeneous catalyst for degradation of organic contaminants. Carbon 60:437–444

[7] Liu Y, Jin W, Zhao Y, Zhang G, Zhang W (2017) Enhanced catalytic degradation of methylene blue by α-Fe2O3/-graphene oxide via heterogeneous photo-Fenton reactions. Appl Catal B 206:642–652

[8] Wang Q, Tian S, Ning P (2013) Degradation mechanism of methylene blue in a heterogeneous fenton-like reaction catalyzed by ferrocene. Ind Eng Chem Res 53(2):643–649

[9] Hu X, Liu B, Deng Y, Chen H, Luo S, Sun C, Yang P, Yang S (2011) Adsorption and heterogeneous Fenton degradation of 17α-methyltestosterone on nano Fe3O4/MWCNTs in aqueous solution. Appl Catal B 107(3–4):274–283

[10] Cao Z-F, Wen X, Chen P, Yang F, Ou X-L, Wang S, Zhong H (2018) Synthesis of a novel heterogeneous fenton catalyst and promote the degradation of methylene blue by fast regeneration of Fe2+. Colloids Surf, A 549:94–104

[11] Wang J, Cao Z, Ren H, Yu C, Wang S, Li L, Zhong H (2020) Reactivation of Fenton catalytic performance for Fe3O4 catalyst: optimizing the cyclic performance by low voltage electric field. Appl Surf Sci 500:144045

[12] Chen F, Xie S, Huang X, Qiu X (2017) Ionothermal synthesis of Fe3O4 magnetic nanoparticles as efficient heterogeneous Fenton-like catalysts for degradation of organic pollutants with H2O2. J Hazard Mater 322(Pt A):152–162

[13] Wang W, Liu Y, Li T, Zhou M (2014) Heterogeneous Fenton catalytic degradation of phenol based on controlled release of magnetic nanoparticles. Chem Eng J 242:1–9

[14] Koo H, Salunke BK, Iskandarani B, Oh W-G, Kim BS (2017) Improved degradation of lignocellulosic biomass pretreated by Fenton-like reaction using Fe3O4 magnetic nanoparticles. Biotechnol Bioprocess Eng 22(5):597–603

[15] Feng Y, Zhang H, Xin B, Wu J (2017) Magnetically recyclable reduced graphene oxide nanosheets/magnetite-palladium aerogel with superior catalytic activity and reusability. J Colloid Interface Sci 506:154–161

[16] Shen J, Li Y, Zhu Y, Hu Y, Li C (2016) Aerosol synthesis of Graphene-Fe 3 O 4 hollow hybrid microspheres for heterogeneous Fenton and electro-Fenton reaction. J Environ Chem Eng 4(2):2469–2476

[17] Zubir NA, Yacou C, Motuzas J, Zhang X, Diniz da Costa JC (2014) Structural and functional investigation of graphene oxide-Fe3O4 nanocomposites for the heterogeneous Fenton-like reaction. Sci Rep 4:4594

[18] Boruah PK, Sharma B, Karbhal I, Shelke MV, Das MR (2017) Ammonia-modified graphene sheets decorated with magnetic Fe3O4 nanoparticles for the photocatalytic and photo-Fenton degradation of phenolic compounds under sunlight irradiation. J Hazard Mater 325:90–100

[19] Boruah PK, Borthakur P, Darabdhara G, Kamaja CK, Karbhal I, Shelke MV, Phukan P, Saikia D, Das MR (2016) Sunlight assisted degradation of dye molecules and reduction of toxic Cr(vi) in aqueous medium using magnetically recoverable Fe3O4/reduced graphene oxide nanocomposite. RSC Adv 6(13):11049–11063

[20] Peng G, Zhang M, Deng S, Shan D, He Q, Yu G (2018) Adsorption and catalytic oxidation of pharmaceuticals by nitrogen-doped reduced graphene oxide/Fe3O4 nanocomposite. Chem Eng J 341:361–370

[21] Shan D, Deng S, Jiang C, Chen Y, Wang B, Wang Y, Huang J, Yu G, Wiesner MR (2018) Hydrophilic and strengthened 3D reduced graphene oxide/nano-Fe3O4 hybrid hydrogel for enhanced adsorption and catalytic oxidation of typical pharmaceuticals. Environ Sci Nano 5(7):1650–1660

[22] Peng S, Zhang D, Huang H, Jin Z, Peng X (2018) Ionic polyacrylamide hydrogel improved by graphene oxide for efficient adsorption of methylene blue. Res Chem Intermed 45(3):1545–1563

[23] Wang H, Gao H, Chen M, Xu X, Wang X, Pan C, Gao J (2016) Microwave-assisted synthesis of reduced graphene oxide/titania nanocomposites as an adsorbent for methylene blue adsorption. Appl Surf Sci 360:840–848

[24] Li Y, Zhang R, Tian X, Yang C, Zhou Z (2016) Facile synthesis of Fe 3 O 4 nanoparticles decorated on 3D graphene aerogels as broad-spectrum sorbents for water treatment. Appl Surf Sci 369:11–18

[25] Hummers W, Offeman RE (1958) Preparation of graphitic oxide. J Am Chem Soc 80:1339

[26] Wei D, Liang J, Zhu Y, Yuan Z, Li N, Qian Y (2013) Formation of graphene-wrapped nanocrystals at room temperature through the colloidal coagulation effect. Part Part Syst Charact 30(2):143–147

[27] Ai L, Zhang C, Chen Z (2011) Removal of methylene blue from aqueous solution by a solvothermal-synthesized graphene/magnetite composite. J Hazard Mater 192(3):1515–1524

[28] Jiang T, Bu F, Feng X, Shakir I, Hao G, Xu Y (2017) Porous Fe2O3 nanoframeworks encapsulated within three-dimensional graphene as high-performance flexible anode for lithium-ion battery. ACS Nano 11(5):5140–5147

[29] Liu H, Jia M, Zhu Q, Cao B, Chen R, Wang Y, Wu F, Xu B (2016) 3D–0D Graphene-Fe3O4 quantum dot hybrids as high-performance anode materials for sodium-ion batteries. ACS Appl Mater Interfaces 8(40):26878–26885

[30] Hu J, Zhang F (2014) Self-assembled fabrication and flame-retardant properties of reduced graphene oxide/waterborne polyurethane nanocomposites. J Therm Anal Calorim 118(3):1561–1568

[31] Peng W, Li H, Liu Y, Song S (2016) Adsorption of methylene blue on graphene oxide prepared from amorphous graphite: effects of pH and foreign ions. J Mol Liq 221:82–87

[32] Wang W, Tian G, Zhang Z, Wang A (2015) A simple hydrothermal approach to modify palygorskite for high-efficient adsorption of Methylene blue and Cu(II) ions. Chem Eng J 265:228–238

[33] Huang R, Fang Z, Yan X, Cheng W (2012) Heterogeneous sono-Fenton catalytic degradation of bisphenol A by Fe3O4 magnetic nanoparticles under neutral condition. Chem Eng J 197:242–249

[34] Xu L, Wang J (2012) Fenton-like degradation of 2,4-dichlorophenol using Fe3O4 magnetic nanoparticles. Appl Catal B 123–124:117–126

[35] Zheng X, Feng J, Zong Y, Miao H, Hu X, Bai J, Li X (2015) Hydrophobic graphene nanosheets decorated by monodispersed superparamagnetic Fe3O4 nanocrystals as synergistic electromagnetic wave absorbers. J Mater Chem C 3(17):4452–4463

[36] Xu X, Li H, Zhang Q, Hu H, Zhao Z, Li J, Li J, Qiao Y, Gogotsi Y (2015) Self-Sensing, Ultralight, and Conductive 3D Graphene/Iron Oxide Aerogel Elastomer Deformable in a Magnetic Field. ACS Nano 9(4):3969–3977

[37] Zhu Y, Murali S, Cai W, Li X, Suk JW, Potts JR, Ruoff RS (2010) Graphene and graphene oxide: synthesis, properties, and applications. Adv Mater 22(35):3906–3924

[38] Ferrari AC, Basko DM (2013) Raman spectroscopy as a versatile tool for studying the properties of graphene. Nat Nanotechnol 8(4):235–246

[39] Chen M, Zhang C, Li X, Zhang L, Ma Y, Zhang L, Xu X, Xia F, Wang W, Gao J (2013) A one-step method for reduction and self-assembling of graphene oxide into reduced graphene oxide aerogels. J Mater Chem A 1(8):2869

[40] Ren L, Huang S, Fan W, Liu T (2011) One-step preparation of hierarchical superparamagnetic iron oxide/graphene composites via hydrothermal method. Appl Surf Sci 258(3):1132–1138

[41] Zong M, Huang Y, Zhao Y, Sun X, Qu C, Luo D, Zheng J (2013) Facile preparation, high microwave absorption and microwave absorbing mechanism of RGO–Fe3O4 composites. RSC Adv 3(45):23638

[42] Yang X, Li Y, Du Q, Wang X, Hu S, Chen L, Wang Z, Xia Y, Xia L (2016) Adsorption of methylene blue from aqueous solutions by polyvinyl alcohol/graphene oxide composites. J Nanosci Nanotechnol 16(2):1775–1782

[43] Mahmoudi K, Hosni K, Hamdi N, Srasra E (2014) Kinetics and equilibrium studies on removal of methylene blue and methyl orange by adsorption onto activated carbon prepared from date pits-A comparative study. Korean J Chem Eng 32(2):274–283

[44] Yao Y, Miao S, Liu S, Ma LP, Sun H, Wang S (2012) Synthesis, characterization, and adsorption properties of magnetic Fe3O4@graphene nanocomposite. Chem Eng J 184:326–332

[45] Fu J, Chen Z, Wang M, Liu S, Zhang J, Zhang J, Han R, Xu Q (2015) Adsorption of methylene blue by a high-efficiency adsorbent (polydopamine microspheres): kinetics, isotherm, thermodynamics and mechanism analysis. Chem Eng J 259:53–61

[46] Liu T, Li Y, Du Q, Sun J, Jiao Y, Yang G, Wang Z, Xia Y, Zhang W, Wang K, Zhu H, Wu D (2012) Adsorption of methylene blue from aqueous solution by graphene. Colloids Surf B, Biointerfaces 90:197–203

[47] Zhou L, Zhang H, Ji L, Shao Y, Li Y (2014) Fe3O4/MWCNT as a heterogeneous Fenton catalyst: degradation pathways of tetrabromobisphenol A. RSC Adv 4(47):24900

[48] Li W, Wu X, Li S, Tang W, Chen Y (2018) Magnetic porous Fe3O4/carbon octahedra derived from iron-based metal-organic framework as heterogeneous Fenton-like catalyst. Appl Surf Sci 436:252–262

[49] Shi X, Tian A, You J, Yang H, Wang Y, Xue X (2018) Degradation of organic dyes by a new heterogeneous Fenton reagent—Fe2GeS4 nanoparticle. J Hazard Mater 353:182–189

[50] Pignatello JJ, Oliveros E, MacKay A (2006) Advanced Oxidation processes for organic contaminant destruction based on the Fenton reaction and related chemistry. Crit Rev Environ Sci Technol 36(1):1–84

[51] Ai L, Jiang J (2012) Removal of methylene blue from aqueous solution with self-assembled cylindrical graphene–carbon nanotube hybrid. Chem Eng J 192:156–163

[52] He J, Yang X, Men B, Bi Z, Pu Y, Wang D (2014) Heterogeneous Fenton oxidation of catechol and 4-chlorocatechol catalyzed by nano-Fe3O4: role of the interface. Chem Eng J 258:433–441

[53] Long M, Qin Y, Tan B, Zhou B (2014) RhB adsorption performance of magnetic adsorbent Fe3O4/RGO composite and its regeneration through a fenton-like reaction. Nano-Micro Letters 6(2):125–135